International Journal of Multiphysics
Volume 18, No. 1s, 2024
ISSN: 1750-9548

Computational Modeling and Simulation of Spherical Shell Structure Construction using Moldless Hydro-Plastic Forming

Yoshikazu Higa[1,a], Yasuyoshi Miyahira[2,b], Hirofumi Iyama[3,c], Ken Shimojima[1,d]

[1]Department of Mechanical Systems Engineering, National Institute of Technology (KOSEN), Okinawa College, 905 Henoko, Nago, 905-2192, Japan

[2]Creative System Engineering Advanced Course, National Institute of Technology (KOSEN), Okinawa College, 905 Henoko, Nago, 905-2192, Japan

[3]Department of Mechanical & Intelligent System Engineering, National Institute of Technology (KOSEN), Kumamoto College, Kumamoto 866-8501, Japan

[a]y.higa@okinawa-ct.ac.jp, [b]ac224508@edu.okinawa-ct.ac.jp, [c]eyama@kumamoto-nct.ac.jp, [d]k_shimo@okinawa-ct.ac.jp

Abstract:

1. Herein, the purpose of this study was to use the perspective of computational mechanics to clarify the effects of differences in the mechanical properties of welding joints, which are used as an initial process in mold-less spherical container molding, on the final molded shape. We scrutinized how factors such as the quantity and placement of explosive charges, alongside the mechanical properties of the joints, influence the final spherical shape. Our results confirm that the pressure generated from 2,4,6-trinitrotoluene (TNT) propagates through water as a shock wave, eventually reaching stainless steel (SUS304) and inducing deformation. Through computational analysis, we derived the following insights:A TNT explosive dosage of 10 g proves optimal for the model.
2. Depending on the position of the explosive charge, convex deformation occurs, with the degree of convexity increasing with the position of the explosive charge.
3. Material heterogeneity stemming from welding joints results in the generation of low pressure.

As a culmination of this computational investigation, we were able to investigate moldless hydro plastic processing, offering valuable insights from a mechanics viewpoint.

Keywords: Moldless hydro-plastic forming, Underwater shock wave, Computational simulation

1. Introduction

The demand for spherical shells is on the rise across automotive and aerospace industries, prompting the exploration and development of numerous manufacturing methods. Conventional spherical shell molding relies on molds, but this method requires specialized molds, thereby elevating the production costs. Therefore, the fabrication of such molds for large spherical shells becomes exceedingly challenging. Conversely, moldless metal plastic forming techniques without using dies have been investigated through experiments [1, 2] and numerical simulations [3, 4], with their usefulness under scrutiny. In particular, the research by the Harbin Institute of Technology group is remarkable, reporting a variety of results ranging from mono- to multilayer structures [5], encompassing spherical and ellipsoidal shells [6], spanning ring-shaped configurations [7], variations in thickness of metal sheet [8]. However, to the best of our knowledge, a gap exists in the existing literature: a comprehensive examination of the mechanical properties inherent in welding joints during fabrication and the amount and location of 2,4,6-trinitrotoluene (TNT) explosives used as a high-pressure source remains unexplored [9].

The objective of this study is to clarify, through a computational mechanics perspective, how variations in mechanical properties of a welding joints resulting from structural pretreatment impact the final shape in moldless metal plastic forming. This process entails symmetric expansion of the initial structure into a sphere shape using underwater shock waves. Herein, a numerical simulation model necessary for comprehending pertinent mechanical phenomena is developed. The effects of differences in TNT explosive volume, eccentricity distance (TNT explosive position), and the unique mechanical properties of welding joints on the final shape of the spherical container are investigated, all from a computational mechanics perspective.

2. Fundamental principles for computational simulation scheme

When numerically analyzing a coupled problem involving the interaction between a flow field and structural deformation, such as when a structure vibrates in a fluid medium, the substantial displacement/deformation of the structural system cannot be ignored as it profoundly affects the flow dynamics. Managing situations where the analysis domain related to the fluid deforms alongside the structural motion is imperative. The Arbitrary Lagrangian Eulerian method (ALE) [10] offers a solution for such problems. In this ALE method, if nodes are fixed in computational space, an Eulerian description is used; alternatively, if nodes move with the fluid particles, a Lagrangian description is used. In general, an intermediate description between the two is determined based on the location in the analysis domain. When dealing with problems coupling a viscous fluid and a structure, a Lagrangian description is used on the surface of an object to account for the no-slip condition, while an Eulerian description is used for boundaries fixed in space [11].

Herein, we use general-purpose finite element analysis commercial software to reproduce moldless metal plastic processing phenomena using underwater shock waves. The calculation model comprises a SUS304 container filled with water and explosives, each expressed and modeled using constitutive equations and state equations introduced in the next section. The simulation utilizes RADIOSS, a part of Altair Engineering's HyperWorks, which is a general-purpose finite element analysis software.

3. Computational modeling and its conditions

Herein, as described in the previous section, we use HyperWorks RADIOSS (Altair®), a general-purpose finite element analysis software, to create and analyze a numerical simulation model of the target moldless metal plastic forming process. The analysis model encompasses TNT, water, and SUS304, arranged as shown in Figure 1, with dimensions in millimeters. For computational efficiency and symmetry considerations, we adopt a regular decagon with a diameter D = 300 mm circumscribed in the *rz* plane, as shown in Figure 1. Thin plates a and b (plate thickness = 2 mm) are joined at point c, with the center of member b aligned with the circumcircle. TNT served as a high pressure source for the origin *O*. In addition, the analysis is performed as a 2D model on the *rz* plane owing to the axisymmetric nature of the model around the *z*-axis.

3.1. Equation of state and Constitutive equation

3.1.1. Constitutive equation for SUS304 and its parameters

The simplified Johnson–Cook equation [12,13] is used as the constitutive equation for stainless steel SUS304, neglecting the thermal and strain-rate effects. The equation is represented as follows:

$$\sigma = a + b\varepsilon_p^n, \tag{1}$$

where a, b, and n are the material constants, as outlined in Table 1.

3.1.2. Equation of state for Water and its parameters

The filling area surrounded by the stainless steel SUS304, acting as the workpiece, is designated for water filling. For the equation of state governing the water within this area, we introduce a polynomial approximation [13], expressed as follows (2).

$$P = C_0 + C_1\mu + C_2\mu^2 + C_3\mu^3 + (C_4 + C_5\mu)E_0\,, \qquad \mu = \rho/\rho_0 - 1 \tag{2}$$

where P on the left-hand side of the equation represents the pressure, a fluid state variable. On the right-hand side, $C_0, C_1, C_2, C_3, C_4, C_5$ are coefficients specific to water, while E_0 is the initial energy per unit volume. ρ and ρ_0 denote the density of water and the reference density, respectively. The material properties of the water introduced into the computational simulation are listed in Table 2.

3.1.3. Equation of state for TNT and its parameters

The pressure generated by the expansion of detonation products from the chemical explosive is determined using the Jones–Wilkins–Lee (JWL) equation of state [14]. This equation defines the pressure P_{JWL} as follows:

$$P_{JWL} = A\left[1 - \frac{\omega}{R_1 V}\right]\mathrm{e}^{-R_1 V} + B\left[1 - \frac{\omega}{R_2 V}\right]\mathrm{e}^{-R_2 V} + \frac{\omega E}{V}\,. \tag{3}$$

Additionally, P_{CJ} denotes the Chapman–Jouguet pressure depending on the initial density ρ_0 of the explosive, calculated as follows:

$$P_{CJ} = \frac{\rho_0 D^2}{\gamma + 1}, \qquad \gamma = \frac{c_p}{c_v}\,, \tag{4}$$

where D is the detonation velocity, and γ indicates the ratio of specific heat at constant volume (c_v) to that at constant pressure (c_p). The JWL parameters for TNT are given in Table 3, while A, B, R_1, R_2, and ω are material constants. V denotes the relative volume of the detonation product, and E is the detonation energy per unit volume, initially set at E_0.

4. Computational results and discussions

4.1. Underwater propagation pressure waves induced by detonation

Figure 2 shows the pressure distribution over time inside the vessel generated by the detonation in water with a TNT quantity of 10 g [2]. The depiction reveals a concentric propagation of high-pressure region from the TNT detonation, which serves as the source of high pressure. These regions ultimately reach the outer shell composed of SUS304. The wavefront reaches the top surface of SUS304, located 150 mm above the center of the high-pressure source where the TNT is placed, in ~80 □s, indicating a propagation velocity of ~1875 m/s in water for the wavefront. This result shows that the high-pressure wavefront induced by the TNT detonation exceeds the speed of sound, confirming its classification as an underwater shock wave. Upon reaching the interface between water and strainless-steel plate, the pressure wave undergoes separation into transmitted and reflected waves at SUS304, with the reflected wave observed propagating through the water. Compared to the stainless-steel plates a and b, which are located equidistant from the high-pressure source, the joint point c is located farther away, as shown in Figure 1. Consequently, the reflected waves originating from point c combine to produce pressure waves in the water that depend on the shape of the joint. Notably, the deformation of the plate becomes pronounced approximately 160 □s after the primary wave reaches the plate. This observation indicates that after the penetration of the underwater shock wave induced by the TNT detonation penetrates, the pressure wave propagating inside the stainless-steel plate causes subsequent deformation, leading to the development and transition into the desired spherical shape. Conversely, the transmitted wave at the water–SUS304 interface, after propagating inside the stainless steel, is again separated into transmitted and reflected waves at the interface between the SUS304 outer wall and its surroundings (but treated as a vacuum in the calculation model). Although the reflected wave contributes to plate deformation as it propagates through the stainless steel, the transmitted wave attenuates rapidly owing to the characteristics of the numerical model, rendering the effect of the reflected wave negligible.

4.2. Effect of explosive amount difference on the final shape

To investigate the effect of different amounts of TNT explosive on the final shape of spherical pressure vessels, a computational model was developed, and numerical simulations were performed with an initial value of ±5 g for the explosive amounts, as detailed in Ref. [2]. In the model with 10 g of TNT, the diameter in the analytical model shown in Figure 1 is 22.72 mm, while the diameters of the 5 and 15 g models correspond to 18.02 and 26.00 mm, respectively. Figure 3 shows the deformation and equivalent stress distribution of a stainless-steel plate at 400 □s. In the models with 5 and 10 g of TNT, the shape appears generally spherical, albeit with varying degrees of deformation. However, in the 15 g TNT model, the deformation is excessive, resulting in a

convex shape at the top and bottom sheet. For each explosive amount, substantial deformation occurs in plates corresponding to a and b shown in Figure 1, while deformation at the joint corresponding to c is minimal. It was found that deformation at welding joints was negligible, with deformation of the stainless-steel plates being predominant, enabling the formation of the desired spherical container. These computational results align with previously reported experimental results [1,2], endorsing the validity of the moldless hydro-plastic forming process from a computational mechanics viewpoint.

4.3. Effect of explosive location difference on the final shape

Figure 4 shows the visualization of deformation in the stainless-steel plate, aiming at its impact on the final shape of the spherical container when the position of the explosive charge is changed. In this figure, the cross ”x” mark indicates the center position of TNT, with each explosive charge amounting to 10 g. Notably, the position of the explosive, serving as the high-pressure source, is shown as eccentrically located from the center, creating a teardrop shape. Furthermore, by eccentrically moving the explosive closer to the stainless-steel plate, the extent of deformation in the convex plate increases. These results suggest the feasibility of unique shaping an ellipsoidal spherical axisymmetric body by changing the amount and position of the explosive, which serves as the high-pressure source.

4.4. Effect of mechanical characteristic difference of welding joint on the final shape

The time histories of the equivalent stress distribution in the stainless-steel plate are shown to investigate the effect of differences in the mechanical properties of joints on the final shape, as shown in Figure 5. Two scenarios were examined for the welding points: (a) the E model, with the same modulus of elasticity as that of the stainless-steel plate, and (b) the 1.1E model, with a 10% increase in the modulus of elasticity. Since stress waves propagate differently in stainless-steel plates owing to variations in the longitudinal elastic modulus, pronounced differences in stress distribution are expected within the stainless-steel plates in the numerical simulation model. However, it was confirmed that there is no notable difference in the equivalent stress distribution during the transition period between 80 and 90 μs, where yield stress occurs in the stainless steel in the numerical simulation model, and around 300 μs when a spherical pressure vessel forms. These results indicate that the contribution of longitudinal elasticity modulus to the deformation of stainless steel is negligible.

In the future, the influence on the final shape should be investigated by introducing a detailed constitutive equation that considers the plastic properties of the joint. This avenue presents a promising direction for future research.

5. Conclusions

Herein, a comprehensive numerical simulation model was developed to investigate the effects of varying detonation charge amounts, detonation charge locations, and mechanical properties of joints on the final shape of the molded metal plasticity. This process involves symmetric expansion and shaping into a sphere shape through underwater shock waves induced by detonation. The results of these numerical simulations show that pressure waves generated by TNT propagate as underwater shock waves in water, leading to plastic deformation along the

in-plane direction of the steel plate upon reaching the stainless-steel plate. Key findings from numerical simulations with varied parameters are as follows:

1. It was confirmed that, for the specified model dimensions, a desired spherical container could be achieved using a 10 g TNT burst, aligning with previously reported experimental results.
2. Differences in explosive position induce convex deformation, with a pronounced convex shape observed when the explosive is closer to the metal sheet.
3. It was confirmed that the equivalent stress distribution in the steel plate, when material heterogeneity is introduced owing to the differences in stiffness at the joint, does not notably differ from the results obtained from simplified numerical simulation model treating the material as homogeneous.

These computational mechanics insights offer valuable knowledge for moldless metal plastic forming. Further modeling of welding joints, as mentioned in point 3, will enhance precision through the introduction of the plastic properties of the joints, representing a promising avenue for future research.

Acknowledgement

The authors gratefully acknowledge financial support from JSPS KAKENHI Grant-in-Aid for Scientific Research (C), 19K12393 and 20K04220.

References

[1] Tiesheng, Z., Zhensheng, L., Changji, G. and Zheng T., Explosive forming of spherical metal vessels without dies, J. Mat. Process. Tech., **31** (1992), 135-145.

[2] Zhang, R. and Zhang, T.-S., Non-die explosive forming of spherical pressure-vessels, J. Mat. Process. Tech., **41** (1994), 341-347.

[3] Hashemi, J., Helm, J. and Sheets, C.L., New method in design and manufacturing of fluid-filled multi-layered spherical pressure vessels, International Journal of Pressure Vessels and Piping, **58**-3 (1994), 355-360.

[4] Zhang, R., Iyama, H., Fujita, M. and Zhang, T.-S., Optimum structure design method for non-die explosive forming of spherical vessel technology, J. Mat. Process. Tech., **85** (1999), 217-219.

[5] Zhang, S.H., Research on integral hydro-bulge forming two layer polyhedron into spherical vessels, Dr. Thesis, Harbin Inst. Tech., (1991)

[6] Song, Y.S., Research on integral hydro-bulge forming polyhedron into ellipsoidal sell, Dr. Thesis, Harbin Inst. Tech., (1996)

[7] Zhang, X., Research on the integrated hydrobulge forming technology of ring shell, Dr. Thesis, Harbin Inst. Tech., (1998)

[8] Wang, F.Z., Research on integral hydro-bulge forming polyhedron with different thickness into spherical vessel, Dr. Thesis, Harbin Inst. Tech., (1997)

[9] Iyama, H., et al., Chap. 2, Explosive forming; Explosion, Shock-wave and High-strain-rate Phenomena of Advanced Materials, A volume in Multiphysics: Advances and Applications (2021), Academic Press

[10] C.W. Hirt, A.A. Amsden and J.L. Cook; An Arbitrary Lagrangian Eulerian Computing Method for All Flow Speeds, J.

Computational Physics Vol.14, No.3 (1974), pp.227-253.

[11] Khawaja, H. and Moatamedi, M., Multiphysics modelling of fruid-particulate systems (Multiphysic: Advances and Applications), Academic Press, (2020).

[12] Johnson, G.R. and Cook, W.H., A constitutive model and data for metals subjected to large strains, high strain rates and high temperatures, Proceedings of the 7th International Symposium on Ballistics, The Hague, The Netherlands, (1983).

[13] RADIOSS theory manual 14.0 version, Large Displacement Finite Element Analysis, Altair Eng., Inc. (2015)

[14] Mader, C.L., Numerical Modeling of Detonations, University of California Press (1979).

Table

Table 1 Mechanical characteristics of SUS304

Density [kg/m^3]	7930
Modulus of elasticity [GPa]	206
Poisson's ratio [-]	0.3
a [MPa]	193
b [MPa]	450
n [-]	0.5

Table 2 Parameters of Water

Density [kg/m^3]	1000
C_0 [MPa]	0
C_1 [MPa]	2199
C_2 [MPa]	5351
C_3 [MPa]	7324
C_4, C_5 [-]	0
E_0 [J/m^3]	0

Table 3 Parameters of TNT explosive

Density [kg/m^3]	1630
A [GPa]	373
B [GPa]	3.74
R_1 [-]	4.15
R_2 [-]	0.95
ω [-]	0.36
D [m/s]	6930
P_{CJ} [GPa]	21.0

International Journal of Multiphysics
Volume 18, No. 1s, 2024
ISSN: 1750-9548

Figure

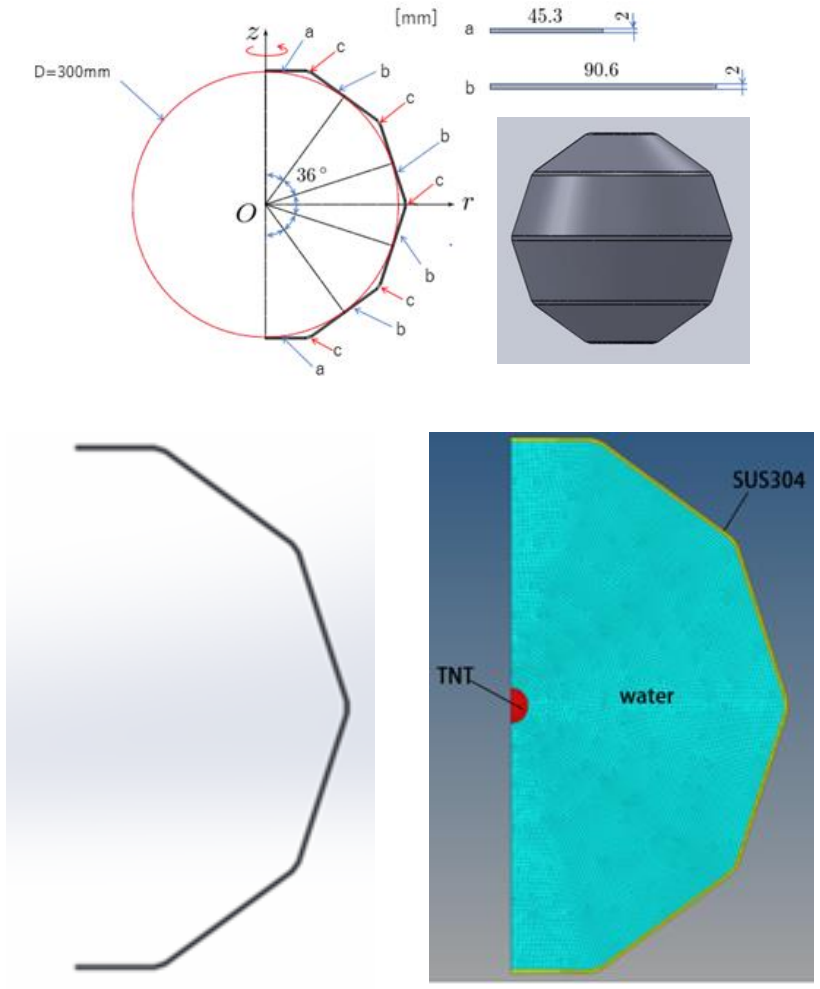

Figure 1 Dimensions and schematic diagram of computational modeling for moldless hydro-plastic forming: a and b denote SUS plate, while c denotes the welding joint

https://doi.org/10.52710/ijm.v18.i1s.1003

International Journal of Multiphysics
Volume 18, No. 1s, 2024
ISSN: 1750-9548

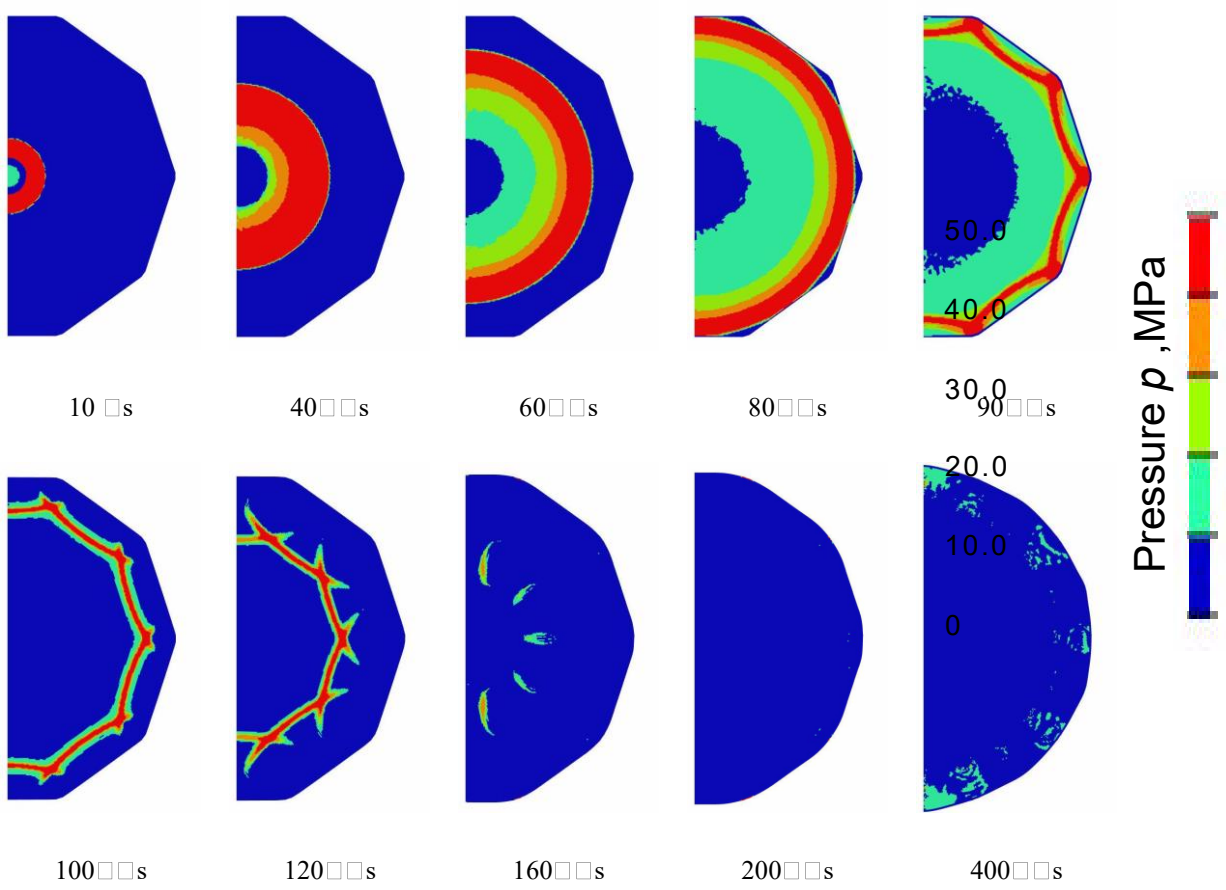

Figure 2 Time history of pressure distribution in the vessel with 10 g of TNT

https://doi.org/10.52710/ijm.v18.i1s.1003

International Journal of Multiphysics
Volume 18, No. 1s, 2024
ISSN: 1750-9548

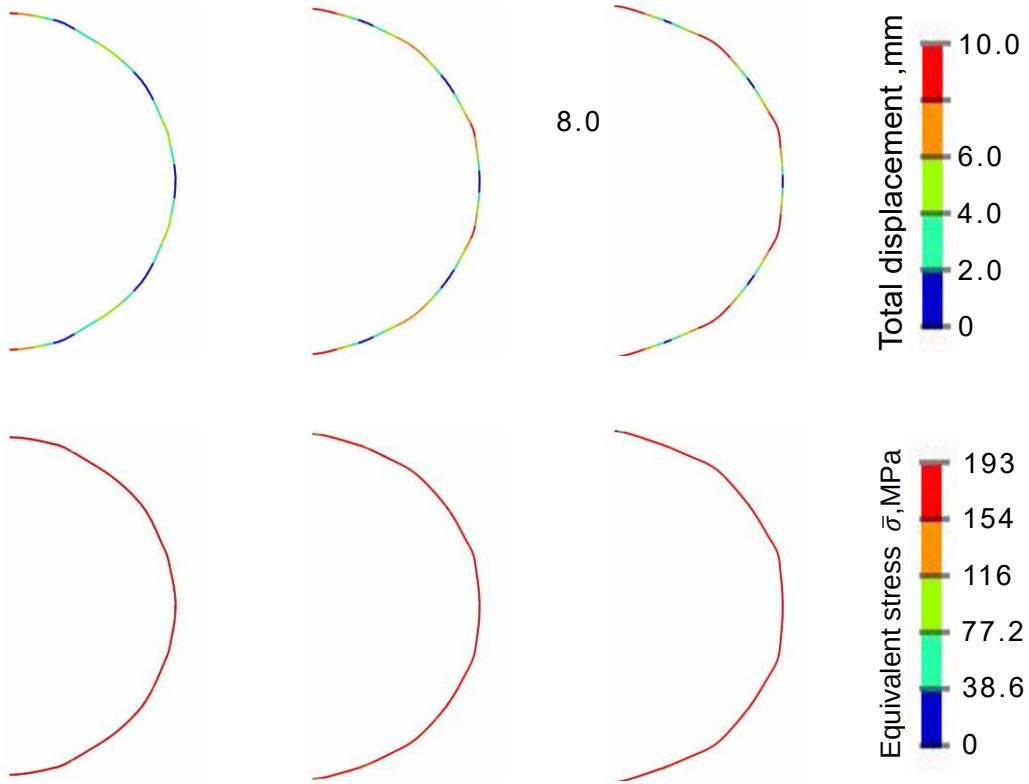

Figure 3 Effect of varying explosive amounts on final shapes at $t = 400$ s; the upper and lower columns depict total displacement and equivalent stress distributions, respectively.

https://doi.org/10.52710/ijm.v18.i1s.1003

International Journal of Multiphysics
Volume 18, No. 1s, 2024
ISSN: 1750-9548

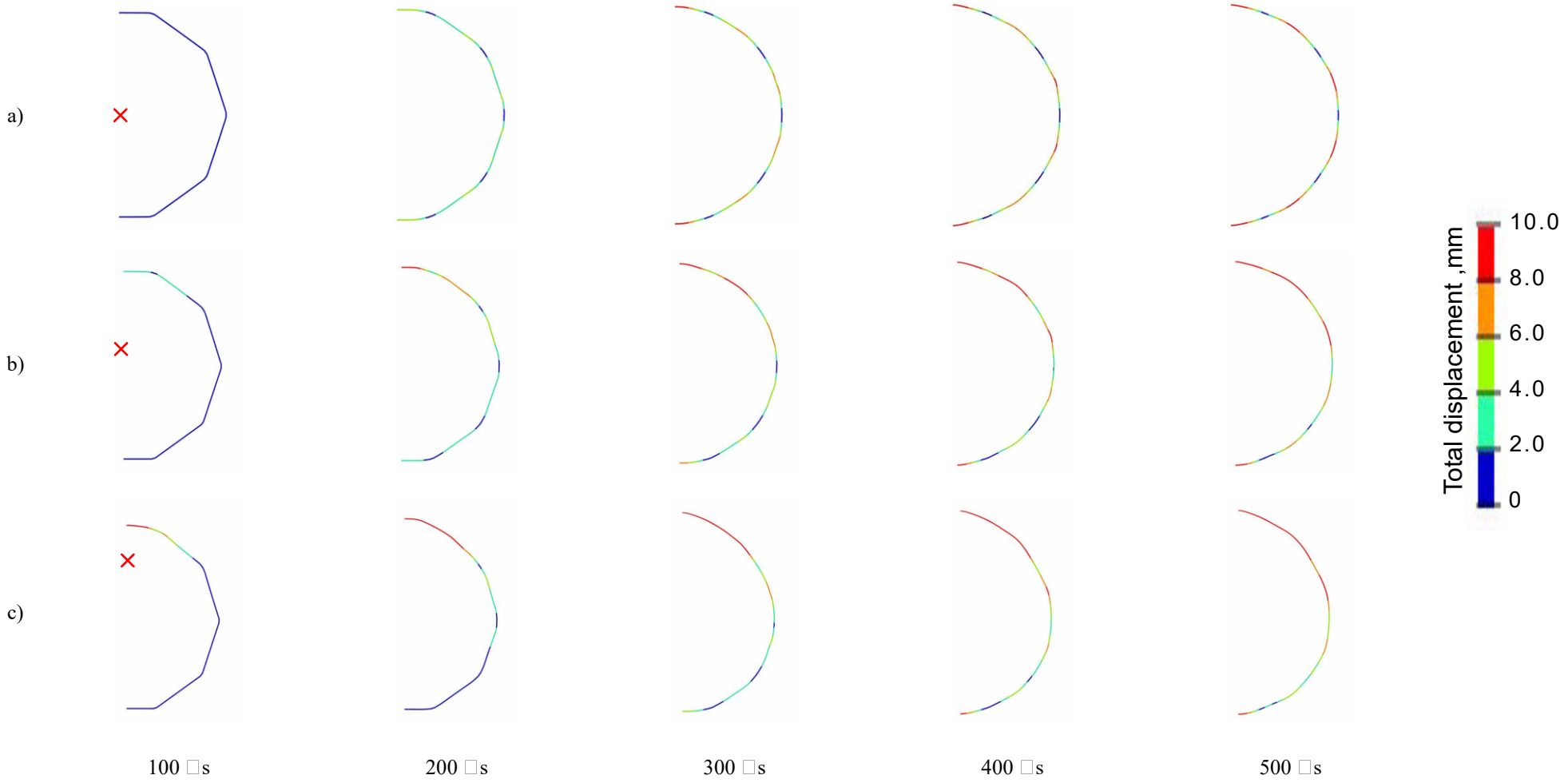

Figure 4 The time history of total displacement at each time step. The cross sign denotes the location of 10 g of TNT: a) center, b) 50 mm, and c) 100 mm shifted from the center.

https://doi.org/10.52710/ijm.v18.i1s.1003

International Journal of Multiphysics
Volume 18, No. 1s, 2024
ISSN: 1750-9548

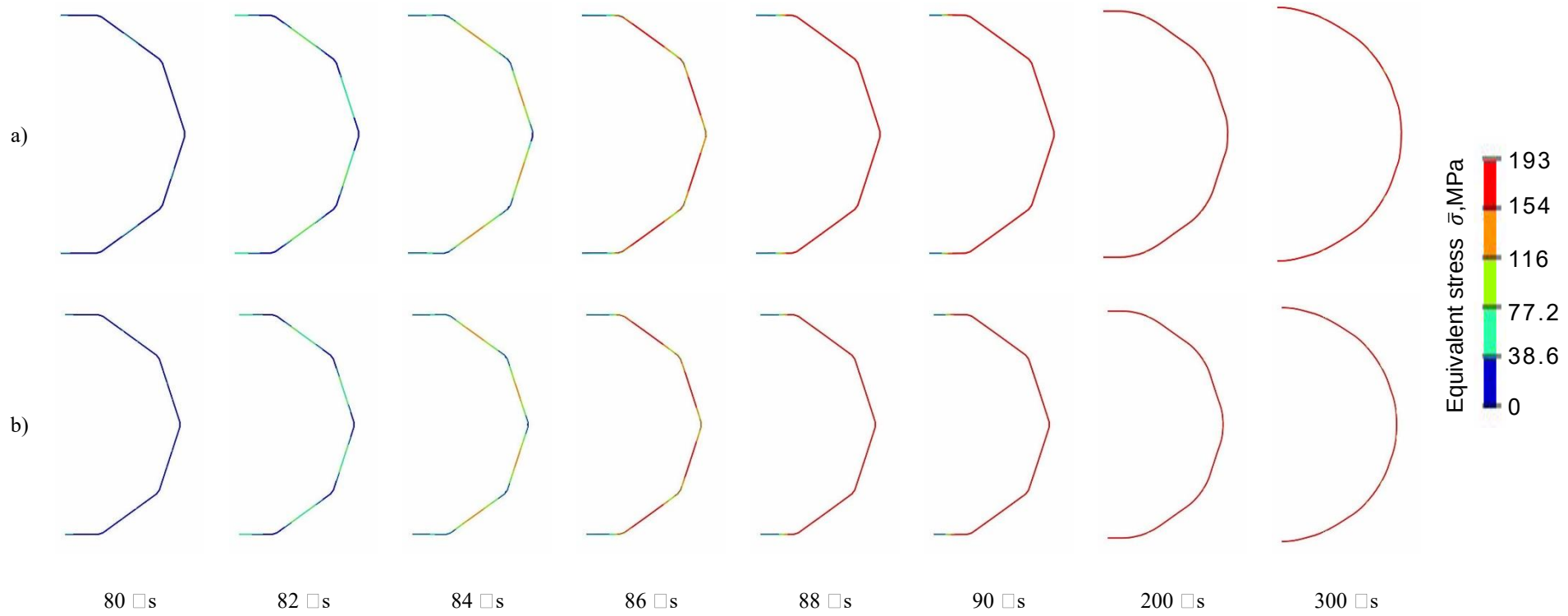

Figure 5 Time history of equivalent stress at each time step. The material parameters of the welding joint: the case of a) elastic modulus E is the same as SUS304 and b) elastic modulus is increased by 10% to 1.1E.

https://doi.org/10.52710/ijm.v18.i1s.1003